Journal of Organometallic Chemistry 839 (2017) 60–70

Contents lists available at ScienceDirect

Journal of Organometallic Chemistry

journal homepage: www.elsevier.com/locate/jorganchem

Redox-active metal complexes with 2,2′-dipicolylamine containing ferrocenyl moiety: Synthesis, electrochemical behavior and biological activity

Elena R. Milaeva [a, b, *], Vladimir Yu. Tyurin [a], Dmitry B. Shpakovsky [a], Anna A. Moiseeva [a], Yulia A. Gracheva [a], Taisiya A. Antonenko [a], Viktoria V. Maduar [a], Dmitry I. Osolodkin [a, c], Vladimir A. Palyulin [a, b], Elena F. Shevtsova [b]

[a] Lomonosov Moscow State University, Department of Chemistry, 119991 Moscow, Russia
[b] Institute of Physiologically Active Compounds of Russian Academy of Sciences, Chernogolovka, Moscow Region, 142432, Russia
[c] Chumakov Institute of Poliomyelitis and Viral Encephalitides, Moscow 142782, Russia

ARTICLE INFO

Article history:
Received 29 November 2016
Received in revised form
15 March 2017
Accepted 18 March 2017
Available online 22 March 2017

Keywords:
Ferrocene
Dipicolylamine metal complexes
Synthesis
Electrochemistry
Biological activity

ABSTRACT

The novel metal complexes of general formula $MCl_2 \cdot \mathbf{L}$ (M = Cu, Fe, Co, Mn, Zn) based on the di-(2-picolyl)amine ligand **L** with the redox-active ferrocenyl fragment were synthesized and characterized by elemental analysis, IR, ^1H, ^{13}C NMR, UV–vis spectroscopy and MALDI-TOF mass spectrometry. The molecular structure of $[ZnCl_2L]$ was established by X-ray crystallography. The redox properties of complexes were studied using cyclic voltammetry (CV) method and feasible schemes of electrochemical transformations were proposed. The antioxidant activity of compounds was tested by various methods. The lipoxygenase (LOX) inhibition activity of the studied compounds was evaluated. The *in vitro* biological experiments were performed using rat brain homogenates. The results demonstrate that ditopic compounds containing ferrocene and redox active dipicolylamine fragments act as polyfunctional antioxidants. These results let us to conclude that combining in one molecule several redox-active metal centers is a promising way of metallodrug design in modern medicinal chemistry.

1. Introduction

The dipicolylamine (DPA) metal complexes are widely used as models of enzymes, metal scavengers, sensors for metal ions and phosphate groups, and in analytical fields (extraction of ions, *etc*) [1–10]. Modification of DPA by introducing moieties with known activity leads to polyfunctional compounds that may be used as pharmaceuticals. A promising approach to incorporate redox-active moiety into biologically active molecules is the application of ferrocenyl fragments [11,12].

In our previous work the Schiff bases of ferrocenecarboxaldehyde bearing 2,6-di-*tert*-butyphenol fragments have been studied by cyclic voltammetry [13].

Recently we have synthesized a series of metal (Zn, Mn, Fe, Co, Ni) complexes of DPA with redox-active 2,6-di-*tert*-butylphenol pendant and the high antioxidant activity was demonstrated [14]. This result opens up the possibility for the design of novel biomimetic systems containing redox-active groups that might serve as electron transfer agents and prevent the oxidative stress.

The oxidative stress occurs when the natural defense systems of the organism are overwhelmed by an excessive generation of reactive oxygen species (ROS), such as superoxide radical-anion $O_2 \cdot^-$, hydroxyl •OH, peroxyl radicals LOO·, lipid hydroperoxides LOOH. It is considered to be involved in many pathological processes, including cardiovascular diseases, mutagenic changes, and cancerogenesis [15–17]. Thus, the development of novel redox-active cell protectors from oxidative stress conditions is of importance. The minimization of negative influence of ROS on living organisms might be achieved by application of compounds with antioxidant activity [18]. There are numerous assays of antioxidant activity based mostly on the ability to quench stable radicals or to change oxidation state of metal-ions [19,20]. For example, a reaction with the stable radical of 2,2'-diphenylpicrylhydrazyl (DPPH) [21–23] and CUPRAC test based on spectrophotometrically

* Corresponding author. Lomonosov Moscow State University, Department of Chemistry, 119991 Moscow, Russia.
E-mail address: milaeva@med.chem.msu.ru (E.R. Milaeva).

http://dx.doi.org/10.1016/j.jorganchem.2017.03.036
0022-328X/

monitored Cu^{2+} ion reduction are widely used [24]. But often there is no correlation between the activity determined by different methods for the same compounds, or even by the same assay in different laboratories [25,26]. Since there is no simple universal method for the accurate and quantitative determination the antioxidant activity the simultaneous application of several assays, such as DPPH-test, CUPRAC, determination of the activity in the reaction with superoxide radical-anion $O_2\cdot^-$*etc.*, is the most perspective approach.

During the last decade, electrochemical methods are more widely applied for antioxidant activity evaluation [27–30]. Moreover, the redox and antioxidant properties are tightly connected [31]. The introduction of appropriate metal ions capable to electron transfer may open new ways for increasing of the antioxidant efficiency of such polyfunctional compounds and elucidate the possible role of redox center in mechanism of this activity. Both redox and antioxidant properties of the complexes with 2,6-di-*tert*-butylphenol pendant on DPA were studied [32] by cyclic voltammetry (CV) and rotating disk electrode (RDE) methods, and it was demonstrated that metal ion plays a key role in mechanism of activity. The most easily oxidized iron complex shows the best antioxidant efficiency in DPPH test that implies the electron transfer step in the mechanism of radical scavenging. In general, data obtained by both spectrophotometrical and electrochemical DPPH-tests correlate. In order to elucidate the role of redox-active moieties in total antioxidant and biological activity, complexes with DPA containing ferrocenylmethyl pendant capable of electron transfer were synthesized (Scheme 1) and their redox properties as well as antioxidant activity were studied in this work.

2. Results and discussion

2.1. Synthesis

Ligand **1** was obtained by reacting ferrocenylmethyltrimethylammonium iodide and 2-dipicolilamine by modified method from Ref. [33]. The reaction was conducted in a small volume of DMF solution instead of water used in Ref. [33], increasing the yield up to 82%. The product extraction required a much smaller amount of diethyl ether than in the case method [33]. Moreover, it significantly reduced the reaction time from 14 h to 2 h by raising the reaction temperature to 115 °C. Structure and purity of the compound **1** was confirmed by IR and NMR spectra.

The complexes **2**–**6** were readily prepared by mixing the metal chlorides and **1** in equimolar ratio in relevant solvents at room temperature or under reflux condition. The compounds were fully characterized by IR, UV–vis, ^{1}H and ^{13}C NMR spectroscopy, MALDI TOF mass spectrometry, and elemental analysis. In MALDI TOF spectra the peaks of two particle types, monomeric ($[L\cdot MCl]^+$) and dimeric ($[(L\cdot M)_2Cl_3]^+$), were observed with stoichiometric metal-ligand ratio **M: L** = 1: 1. The absence of complexes of another composition is connected probably with the large size of ferrocenyl fragment bonded to N-atom.

Among the complexes, only zinc complex **6** is diamagnetic, thus possible to be characterized by NMR (^{1}H, ^{13}C). The signals of ferrocenyl fragment protons remained almost unchanged in the ^{1}H NMR spectrum of **6**, in comparison to the ones of **1** where the signals of the pyridine rings are shifted to the weak field due to electron density transfer from the N atom to zinc. Dramatic changes in the position of methylene group protons have been also observed. Two CH_2 groups associated with the pyridine fragments and two methylene group protons associated with the ferrocene moiety are non-equivalent, in contrast to the free ligand, indicating the limitation of internal rotation of five-membered rings formed upon the metal coordination.

2.2. Crystal structure of 6

The molecular structure of [$ZnCl_2$**L**] **6** determined by X-ray diffraction is presented at Fig. 1A. All three distances Zn–N are very close (2.1763 Å and 2.1788 Å – distances to pyridine N atoms, 2.2058 Å – distance to amino group N atom), pointing out the three-dentate coordination of zinc by ligand's three N atoms. The crystal elementary cell includes four densely packed molecules (Fig. 1B). The coordination number of Zn is 5. It could be also seen that the pyridine rings are not equivalent due to specific orientation of ferrocenyl fragment in the crystal: it is turned towards one of the pyridine rings to form stacking interactions. In the NMR spectrum this asymmetry is not observed, because in the solution the position of ferrocene is not fixed. Selected bond distances and angles for the complex are given in Table 1, and crystal data, the structure refinement details and elementary crystal cell of complex **6** are given in Supporting Materials (Appendix A. Table S1, Fig. S1).

2.3. Vibrational spectroscopy

All compounds obtained have been characterized by IR spectroscopy. In the spectrum of **L** there are characteristic stretching bands of CH (3045-3082 cm^{-1}) and CH_2 groups (2838-2929 cm^{-1}), and bands of deformation vibrations of aromatic rings (1566, 1587

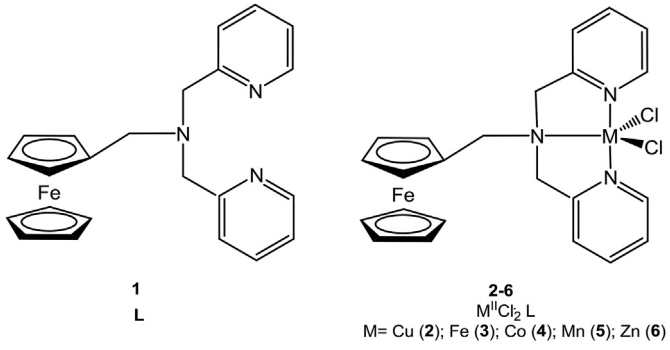

Scheme 1. The structures of 2,2'-dipicolylamine containing ferrocenyl moiety (**L**) and metal complexes based on it.

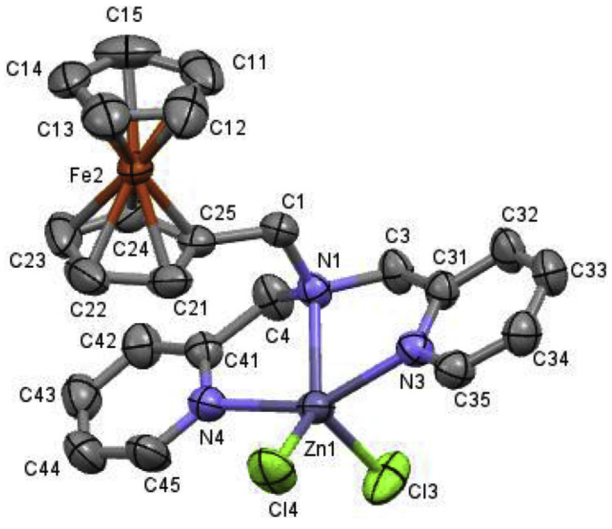

Fig. 1. Thermal displacement ellipsoid (50% probability) plot of **6** with the atom numbering scheme. Hydrogen atoms are omitted for clarity.

Table 1
Selected bond lengths (Å) and angles (°) for complex **6**.

Bond lengths (Å)		Angles (°)	
Zn1–Cl3	2.2851 (10)	Cl3–Zn1–Cl4	116.44 (4)
Zn1–Cl4	2.2510 (11)	Cl3–Zn1–N1	103.32 (6)
Zn1–N1	2.199 (2)	Cl3–Zn1–N3	95.68 (6)
Zn1–N3	2.175 (2)	Cl3–Zn1–N4	97.57 (7)
Zn1–N4	2.178 (3)	Cl4–Zn1–N1	140.24 (6)
		Cl4–Zn1–N3	99.23 (7)
		Cl4–Zn1–N4	97.96 (7)
		N1–Zn1–N3	75.71 (8)
		N1–Zn1–N4	75.95 (8)
		N3–Zn1–N4	150.79 (8)

cm-1). In the IR spectra of complexes **2**–**6** these bands are slightly shifted compared to the corresponding free ligand bands, being an evidence of complex formation.

2.4. Electronic spectra

Ferrocene derivatives are colored both in solution and in the solid state. The spectral data (λ and ε) of the compounds **1**–**6** solutions in MeOH and CH_2Cl_2 are presented in Table 2. The spectra of the compounds **1**–**6** have the intense bands at 253–262 nm, but the molar absorption varies from 6309 to 15849 M cm^{-1} for the different compounds. These bands have a complicated profile due to the superposition of several bands of electronic transitions in the ferrocene core of the molecule and the transition of the pyridine moiety allowed due to symmetry.

Absorption spectra of copper complex **2** were recorded at different pH, using the constant ionic strength created by 1 M $NaClO_4$ methanol-water solution. Appearance and enhancement of the band at 630 nm shows that ferrocene moiety is oxidized by atmospheric oxygen to the ferrocenium ion in the acidic medium [34–36].

2.5. Redox behavior of compounds

The redox properties of compounds **1**–**6** were studied by cyclic voltammetry (CV) on glassycarbon (GC) electrode in CH_3CN. The experimental redox potential data referred to Fc/Fc^+ couple (E = 0.5/0.43 V vs Ag/AgCl/KCl) are summarized in Table 3, and vs Ag/AgCl (see Table S3a, Appendix A).

Fig. 2 displays CV of compound **1** on GC-electrode. It can be seen that the ligand **1** undergoes three-step oxidation on GC surface (Fig. 2). First one-electron reversible peak obviously corresponds to ferrocene fragment oxidation (see Fig. S2a, Appendix A). The second one at more positive potential of E^{ox} = 0.85 V vs Fc/Fc^+ is irreversible, but the reduction peak of product formed in Step 2 is observed on reverse scan (E = 0.13), pointing out the ECE mechanism. The third peak of oxidation is also irreversible. Such a cascade reactions may be related to anodic reactions of aliphatic tertiary amines containing acidic hydrogen atoms in the α position [37]. The second peak is assigned to the ligand N-centered oxidation which

Table 3
The redox potentials values of **1**–**6** obtained on GC electrode (referenced to Fc/Fc^+ couple).

Compound	E^{ox} (V)			E^{red} (V)		
	E^{ox}_1	E^{ox}_2	E^{ox}_3	E^{red}_1	E^{red}_2	E^{red}_3
1 L	0.00/-0.1	0.85/0.13	1.21[a]		−2.53[a]	–
2 [$CuCl_2$**L**]	0.13/0.05	–	–	−0.6/-0.5	−1.14/-0.79	−1.8[a]
3 [$FeCl_2$**L**]	−0.12/-0.33; −0.62	0.08/0.07	–	- 2.2[a]	–	–
4 [$CoCl_2$**L**]	0.09/0.08	0.78[a]	–	−1.91	−2.14[a]	–
5 [$MnCl_2$**L**]	0.09/0.08	0.64/0.55	0.94[a]		−2.47	–
6 [$ZnCl_2$**L**]	0.09/0.08	1.4[a]	–	−2.54	–	–

[a] Irreversible.

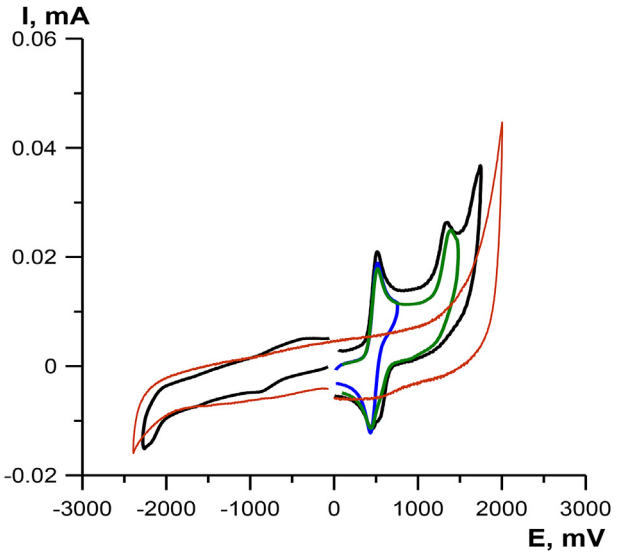

Fig. 2. CV curve of $1 \cdot 10^{-3}$ M compound **1** on GC electrode (200 mV/s, $TBABF_4$, Ag/AgCl, CH_3CN; red line -solvent without additives). (For interpretation of the references to colour in this figure legend, the reader is referred to the web version of this article.)

proceeds through the intermediacy of a nitrogen-centered radical cation which is deprotonated and further oxidized to an iminium ion according to Scheme 2. Eventually, these species can be hydrolyzed by traces of water to yield the corresponding aldehyde and secondary amine. The H^+ liberated in the step 2 is able to protonate the starting compound **1** forming an electroinactive ammonium species (Scheme 2b). According to [38], the reduction peak of low intensity on the reverse scan may be associated with Fc/Fc^+ reduction of iminium cation.

The CV exhibits a peak in cathodic range at $E_{pc} = -2.1$ V, that in agreement with [39] may be attributed to pyridine reduction. But the definite assignment of its nature requires additional studies and is beyond this study.

CV of **2**–**6** display peaks at the potential range 0.08–0.13 V, corresponding to reversible ferrocene–ferrocenium Fc/Fc^+ pair

Table 2
Electronic spectra of compounds **1**–**6**.

Compound	λ_{max}, nm (lgε), C_2H_5OH	λ_{max}, nm (lgε), CH_2Cl_2
1	262.0 (4.1); 432.0 (2.3)	229.0 (3.9); 257.0 (3.9); 436.0 (2.2)
2	259.0 (4.2); 442.5 (2.3); 677.5 (2.3)	229.5 (4.2); 258.0 (4.2); 462.5 (2.4); 763.0 (2.4)
3	253.5 (4.1); 375.5 (3.4)	255.5 (4.0); 385.5 (3.3)
4	257.5 (4.2); 591.5 (2.4)	228.0 (4.0); 256.5 (3.9); 418.5 (2.2); 523.0 (2.2); 557.5 (2.2); 636.5 (2.1)
5	261.0 (4.1); 428.5 (2.3)	227.5 (4.0); 262.5 (4.0)
6	262.0 (4.1); 428.5 (2.4)	228.0 (3.7); 262.0 (3.8); 432.0 (2.3)

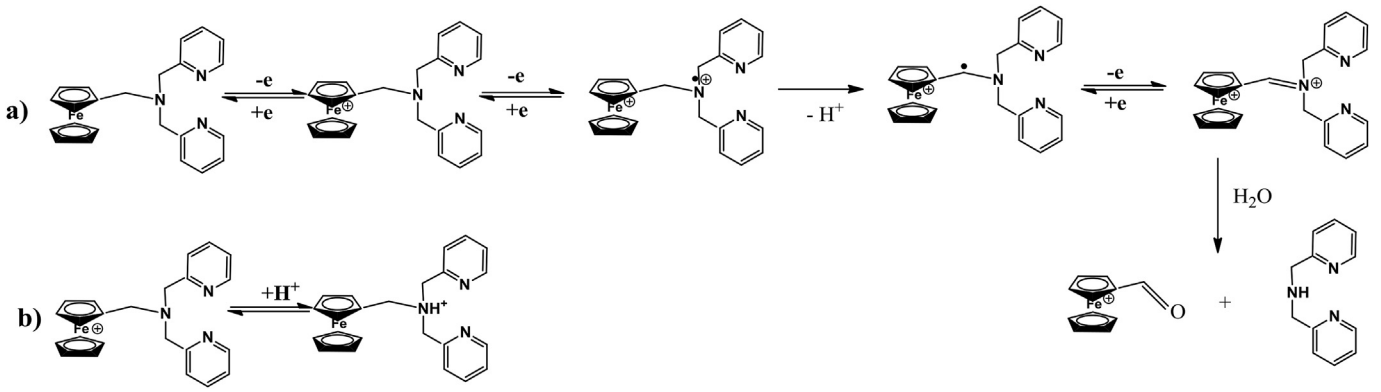

Scheme 2. The redox transformations of ligand **1**.

(Fig. 3). The E_{pa} values of Fc/Fc^+ transition move to more positive values compared to **1**, indicating that the ferrocene centers become more resistant to oxidation, probably due to acceptor effect of positively charged metal ion.

The peak of the amino group oxidation in the copper complex **2** is not observed on GC electrode (Fig. 3). There is a Cu^{II}/Cu^{I} reversible reduction peak (Scheme 3) in the cathodic region, in agreement with the data of [33]. Since the Cu^{I} complex is generally poorly soluble in CH_3CN [40], the second peak at E = - 1.14 V (vs Fc/Fc^+) corresponding to the reduction $Cu^{I} \rightarrow Cu^{0}$ has a low intensity (Fig. 3). When this process occurs, the black precipitate appears on the electrode surface. On the reverse scan after this potential, two peaks are observed: the $Cu^{0} \rightarrow Cu^{II}$ oxidative desorption peak of characteristic triangular shape, and peak corresponding to the transition $Cu^{I} \rightarrow Cu^{II}$. These features on anodic branch appears at reverse scan after potential of Cu^{0} precipitation, on modified electrode surface, that results in the significant increase in current (Fig. 3, black line). We suppose that this also is the reason of the significant shift of ligand **1** reduction peak to anodic potential values (E^{red}_3 = - 1.37 V vs Fc/Fc^+ couple). As it was shown earlier [41,42] the spontaneous reduction process $Cu^{II} \rightarrow Cu^{I}$ might take place if the ligands contain donor atoms and solvent has the nitrile group. We might to propose that the feature at −0.25 V (vs Fc/Fc^+) is associated with the oxidation of such spontaneously reduced Cu^{II} in new ligand environment.

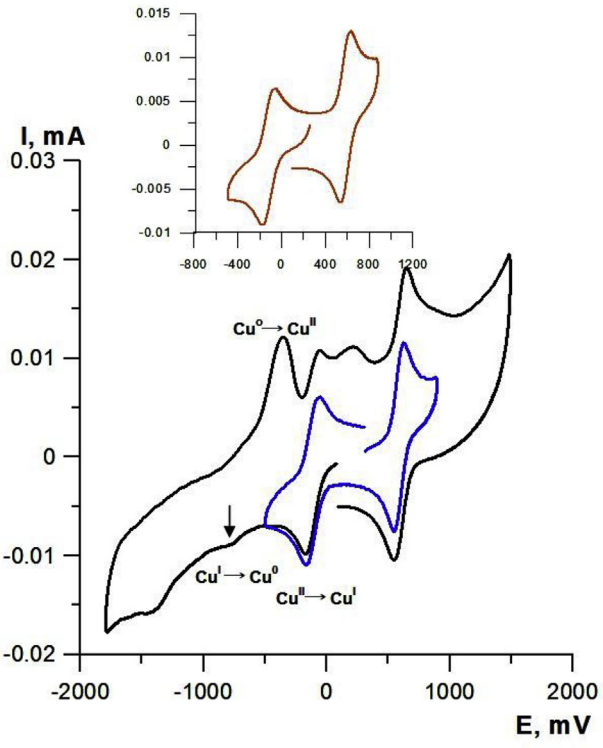

Fig. 3. CV curve of $1 \cdot 10^{-3}$ M compound **2** on GC electrode (200 mV/s, $TBABF_4$, Ag/AgCl, CH_3CN).

The CV of the Fe complex **3** (GC-electrode) displays two oxidative peaks (Fig. 4). The first wave is quasireversible and may be attributed to the $Fe^{II} \rightarrow Fe^{III}$ transition at E = - 0.12 V vs Fc/Fc^+ (the potential of a peak on reverse scan is - 0.33 V). Quasireversibility of this peak may be explained by the geometry change of ligand environment. Second reversible peak corresponds to the ferrocenium fragment oxidation Fc/Fc^+ (Scheme 4). The oxidation peak of amino group is not observed up to the discharge potential of the supporting electrolyte molecules apparently due to the acceptor effect of Fe^{III} ion coordinated with N- atoms.

Another interesting feature of the electrochemical behavior of compound **3** is that the two reduction peaks appear on the reverse scan at more negative potentials than transition Fc^+/Fc. The first one should correspond to the reduction $Fe^{III} \rightarrow Fe^{II}$ at E^{red}_1 = - 0.33 V (vs Fc/Fc^+) in the complex with a modified geometry (quasireversible wave, Fig. 4). The second peak at $E^{red}_2 = -0.62$ V may be attributed to the same reduction of Fe^{III}, but in this case in the complex **3** with a modified ligand environment (It is putative the coordination of acetonitrile, Scheme 4).

The anodic oxidation of Co, Mn, Zn complexes proceeds only with partition of the ligand fragment. The CV of the Co complex **4** on the GC-electrode displays two peaks (Fig. 5a) corresponding to the oxidation of ferrocene fragment (reversible) and amino group by the EC mechanism. In the case of the Mn complex **5** the oxidation of ligand on GC electrode proceeds according to Scheme 2a (Fig. 5b). Three peaks of oxidation are observed in the anode region, the second one responsible for the oxidation of the amino group has some degree of reversibility. The CV of Zn complex **6** on the GC electrode displays two peaks at anodic region (second one is irreversible, implemented the EC-mechanism) (Fig. 5c).

The peak of metal ion reduction is observed on CV of complex **4** in cathodic region. The quasireversible character of the $Co^{II} \rightarrow Co^{I}$ reduction peak at −1.91 V points out the change of complex geometry. At more negative potentials the peak of the ligand reduction appears. In the case of **5** and **6** only peaks of ligand reduction are observed at cathodic potentials (Table 3).

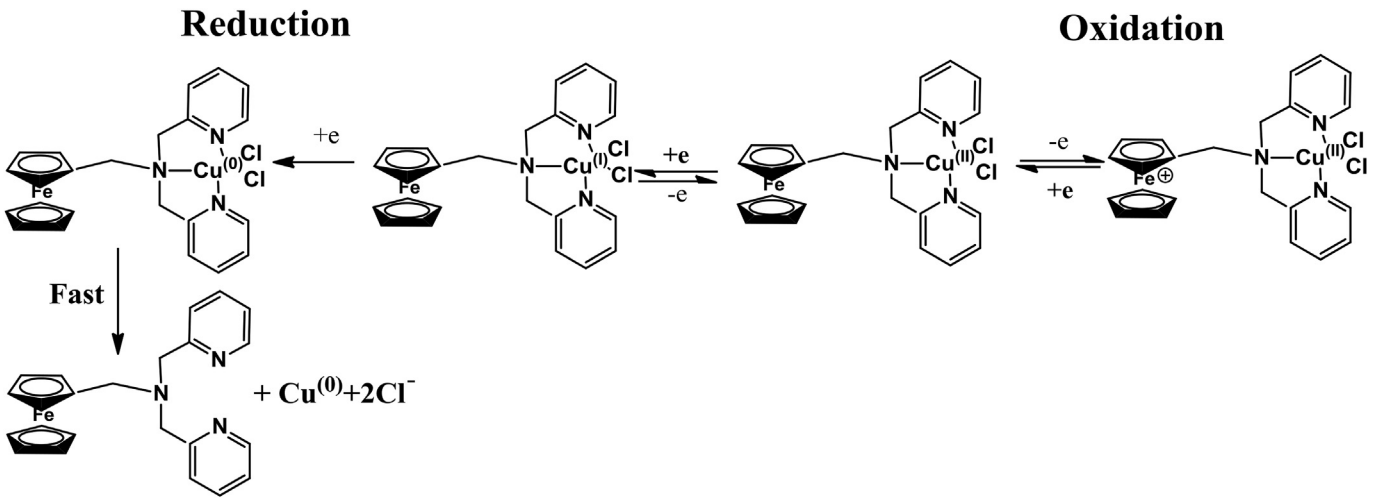

Scheme 3. The redox transformations of Cu complex **2**.

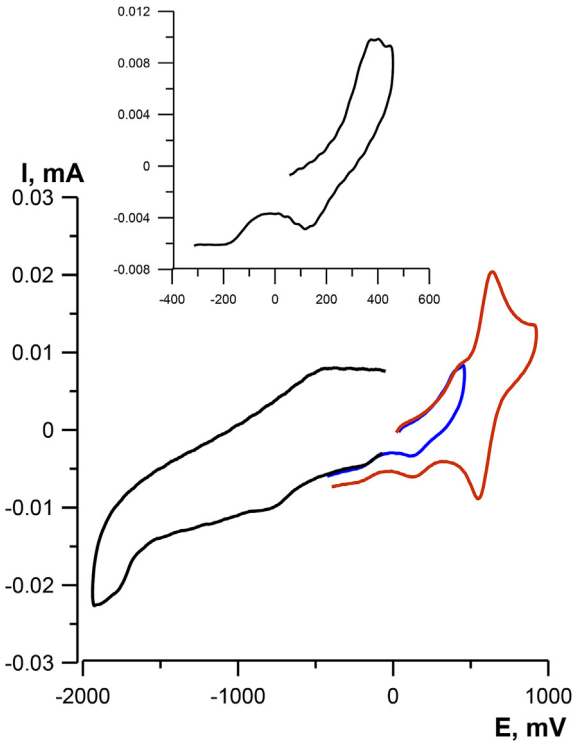

Fig. 4. CV curve of $1 \cdot 10^{-3}$ M compound **3** on GC electrode (200 mV/s, $TBABF_4$, Ag/AgCl, CH_3CN).

2.6. The antioxidant activity study

A series of experimental techniques was used to evaluate the antioxidant activity, namely: DPPH test, CUPRAC test, activity assessment in the reactions with hydrogen peroxide, hydroxyl radical OH, assessment on the activity of non-enzymatic oxidation of linoleic acid (LA) and lipoxygenase (LOX-1B) and activity assessment in the reaction with superoxide radical anion $O_2 \cdot^-$. The results are given in Table 4.

2.7. DPPH test

The activity of radical scavengers was evaluated using the method based on the ability of the compounds to interact with the stable radical 1,1-diphenyl-2-picrylhydrazyl (DPPH) [23]. As can be seen in Table 4, the ligand **L** and most of complexes are weak radical scavengers. The most easily oxidized complex **3** demonstrates highest activity (EC_{50} 44.5 μM) that might be explained by involvement of electron transfer in DPPH reaction. In earlier studies of dipicolylamine complexes containing 2,6-di-*tert*-butylphenol groups, the Fe complex also demonstrated highest activity in spectrophotometric and electrochemical DPPH tests [14,32].

2.8. Cu^{2+} ion reducing (CUPRAC) assay

Compounds **1**–**6** are more potent in CUPRAC test than their analogues containing 2,6-di-*tert*-butylphenol moieties [14], probably due to their redox-active ferrocene fragment capable of Cu^{II} reduction. The results are presented in Trolox equivalents (TEAC, Trolox Equivalent Antioxidant Capacity). TEAC for **2**–**6** was above 0.1, suggesting a key role for metal atom in multifunctional system participating in the copper reduction process. Compound activity increases as follows: **6 (Zn)** < **2 (Cu)** < **3 (Fe)** < **1 (L)** < **4 (Co)** < **5 (Mn)**, and the redox inactive zinc complex **6** is the least active, confirming this hypothesis. Thus, the DPA complexes with ferrocenyl moieties are efficient electron donors.

2.9. Superoxide radical anion scavenging activity

Free radicals are generated *in vivo* by the action of oxidoreductases and oxidases enzymes. For example, superoxide radical anion $O_2 \cdot^-$ is generated by Mo containing xanthine oxidase (XO). The products of O_2 one-electron reduction are ROS ($O_2 \cdot^-$, H_2O_2,•OH), which are involved in the initiation of lipid peroxidation (LP). Xanthine oxidase catabolizes purines to uric acid and regenerates oxygen to superoxide in a conjugate reaction, which immediately dismutates to hydrogen peroxide [43]. Thus, during the reaction active oxygen species capable to cause oxidative stress are formed. The superoxide radical-anion scavenging activity of the complexes was determined by NBT assay [44]. In this method $O_2 \cdot^-$ generated by the xanthine–xanthine oxidase (X–XO system) reduces yellow nitro blue tetrazolium (NBT) to the blue formazan, which is measured spectrophotometrically at 560 nm. Therefore, compounds can compete with NBT for oxidation of the generated superoxide radical-anion. Scavengers are able to inhibit the formation of blue formazan.

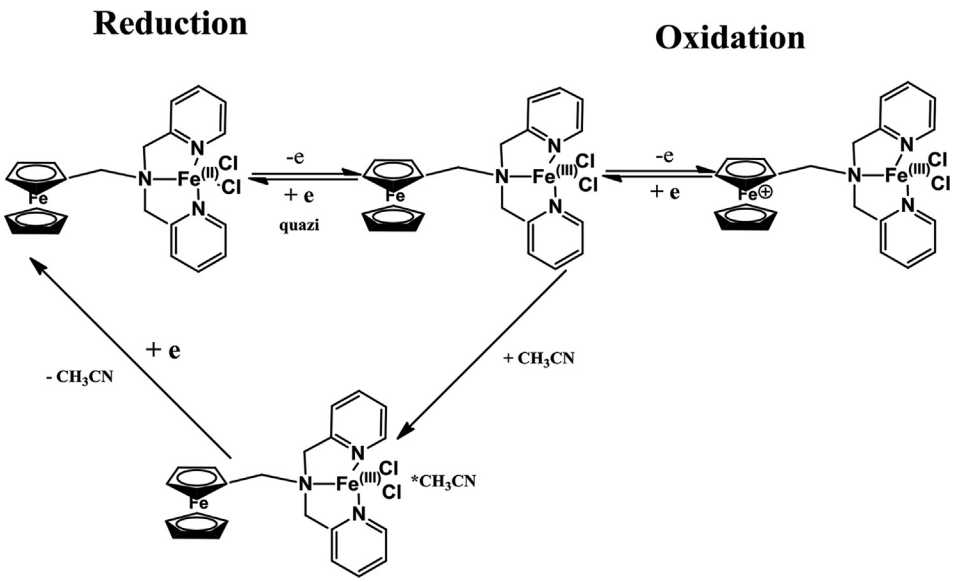

Scheme 4. The redox transformations of Fe complex **3**.

Ligand **L** was found to be inactive in the formation and utilization of the superoxide radical anion, whereas metal complexes **2**–**6** are efficient. The Mn (IC_{50} = 73.5 μM), Cu (IC_{50} = 72.0 μM) and Co (IC_{50} = 28.3 μM) complexes demonstrate high activity in this test. It is of interest that the redox active Fe complex **3** accelerates the formation of blue formazan, which is apparently due to the reduction of NBT to formazan by the ion Fe^{2+} action.

2.10. Hydrogen peroxide test

One of the active oxygen species is H_2O_2 produced in the body tissues from $O_2\cdot^-$, therefore the antioxidant compound should be able to neutralize the H_2O_2 efficiently. Most compounds showed sufficient activity in hydrogen peroxide decomposition. The ligand **L** is the most potent (EC_{50} = 79.5 μM) in the tested series, whereas the EC_{50} values of **2**–**6** are higher (151.2–177.4 μM). Thus, the activity of these compounds against H_2O_2 is primarily confined to the ligand's redox-active ferrocenium center.

2.11. Hydroxyl radical test

Hydroxyl radical ·OH is a reactive dioxygen metabolite, as well as hydrogen peroxide. All the compounds showed a weak activity against··OH: even at the concentration of 2 mM they were able to react less than 50% of hydroxyl radical.

2.12. Inhibition of non-enzymatic peroxidation of linoleic acid

Polyunsaturated fatty acids are fragments of the cell membrane phospholipids and undergo oxidative destruction by ROS causing the membrane damage [7]. The model reaction of linoleic acid (LA) peroxidation in the presence of **1**–**6** was studied. Most compounds have shown low activity and inhibit LA peroxidation by less than 50% at a concentration of 2 mM. The copper complex **2** is the most active.

2.13. Lipoxygenase inhibition

Lipoxygenase (LOX-1B) is an enzyme catalyzing the polyunsaturated fatty acids oxidation. Active oxygen metabolites capable to cause oxidative stress are by-products of this process [45]. Parameter characterizing the compound activity as a lipoxygenase inhibitor is IC_{50} – concentration of compound required to reduce the initial rate of linoleic acid oxidation by 50%.

Change of the LA oxidation rate by LOX-1B and different concentrations of Co complex **4** is shown in Fig. 6. The complexes **2**–**6** demonstrate higher activity than the ligand **1** (**L** does not influence the reaction even at the concentration of 100 μM). The activity of compounds increases in the order **1(L)** << **6** (**Zn**) < **5** (**Mn**) < **3** (**Fe**) < **4** (**Co**) < **2** (**Cu**), suggesting that the metal ion plays a key role in the enzyme inhibition.

The inhibition of lipoxygenase is completely reversible in all cases. When adding linoleic acid to the enzyme incubated with the inhibitor, the reaction rate does not differ from the rate in the absence of incubation. The most efficient inhibition of LOX-1B is achieved by **2** with IC_{50} < 1 μM. The kinetics of LOX-1B inhibition in presence of zinc complex **6** was studied earlier [46].

Possible interactions between the complexes and the enzyme were analyzed with the help of molecular docking. The most energetically favorable binding mode of **6** is shown in Fig. 7. Contrary to the crystal structure, the docked molecule is almost symmetric, and crystal-like conformation is not found among reasonable docking poses. Steric complementarity to the fatty acid binding site of LOX-1B suggests possible competitive interaction. The bidentate ligand **L** cannot accept a favorable conformation similar to the conformation of the complex **6** in the absence of the metal. As soon as there are no directed interactions between the docked molecule and the protein, such as hydrogen bonds, shape complementarity may be the main driving force of the binding. Most LOX-1B substrates are fatty acids, so the binding site is mostly hydrophobic. Iron atom in the binding site may interact with a pyridine ring π system.

2.14. Influence of complexes on lipid peroxidation in rat brain mitochondria

Mitochondria play a crucial role in the functioning of cells: they are the energy factories, where the synthesis of ATP, coupled with the O_2 to H_2O reduction, proceeds. Thus, mitochondria are the major site for generating free radicals, including active oxygen metabolites. The effect of compounds **1**–**6** on lipid peroxidation (LP) in isolated brain mitochondria of Wistar rats was studied using

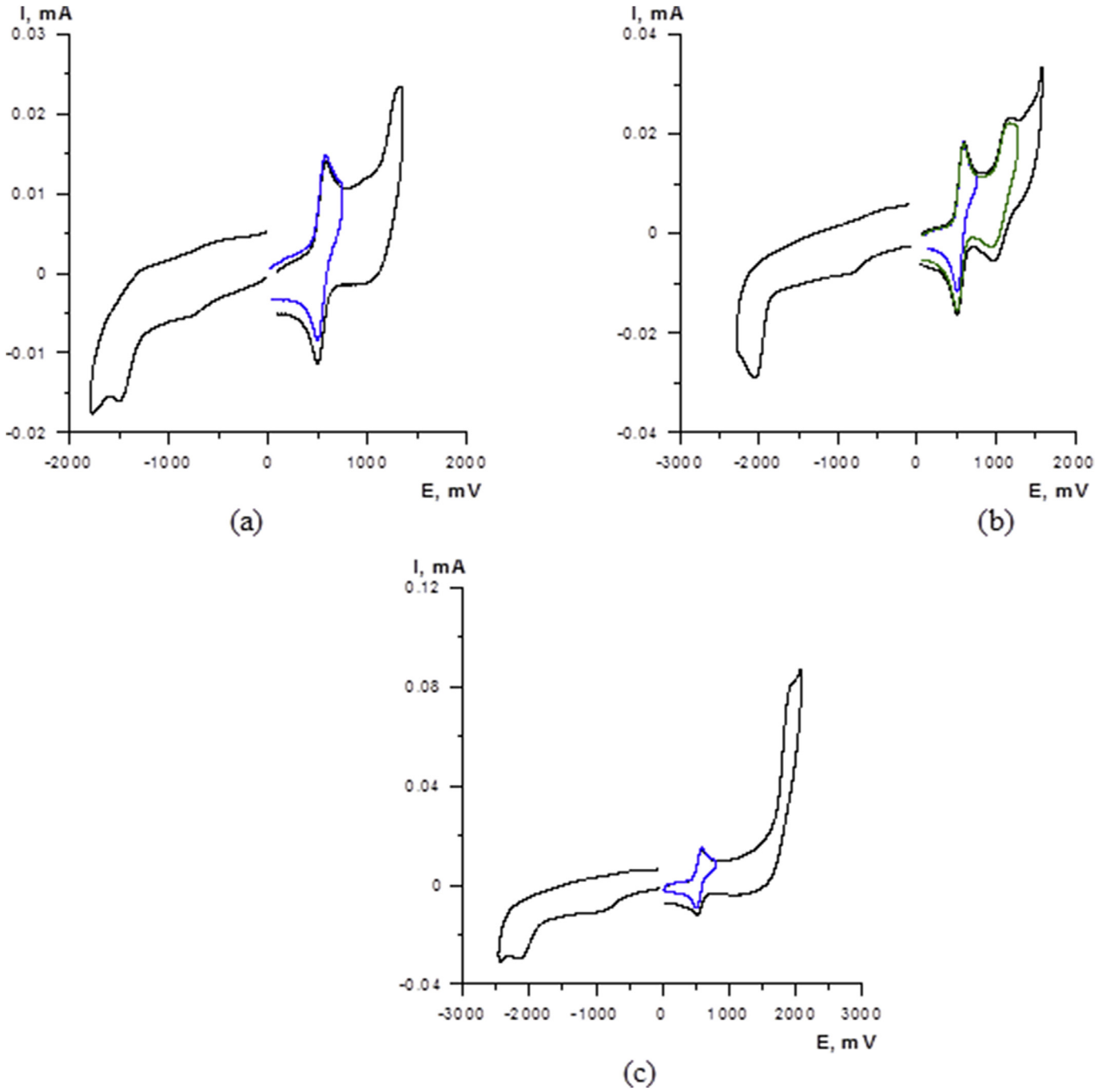

Fig. 5. CV curves of $1 \cdot 10^{-3}$ M compounds **4**–**6** on GC electrode: (a) **4**, (b) **5**, (c) **6** (200 mV/s, $TBABF_4$, Ag/AgCl, CH_3CN).

Table 4
Antioxidant activity of compounds **1**–**6**.

Method	**1** (L)	**2** (Cu)	**3** (Fe)	**4** (Co)	**5** (Mn)	**6** (Zn)
DPPH, EC_{50}, μM	>1000	>1500	44.5	414	>1000	467
CUPRAC, TEAC	0.21	0.16	0.18	0.23	0.47	0.13
H_2O_2 decomposition, EC_{50}, μM	80	151	168	164	–	177
•OH scavenging activity, (%)[a]	42	14	21	11	25	3
Inhibition of LA peroxidation (%)[a]	35	64	8	41	29	–
Inhibition of LOX-1B, IC_{50}, μM	>100	0.9	9	5	13	14
$O_2 \cdot^-$, scavenging activity IC_{50}, μM	[b]	72	activation	28	73	–

[a] The percentage of inhibition at the compound concentration of 2 mM.
[b] Not determined due to inactivity of compound.

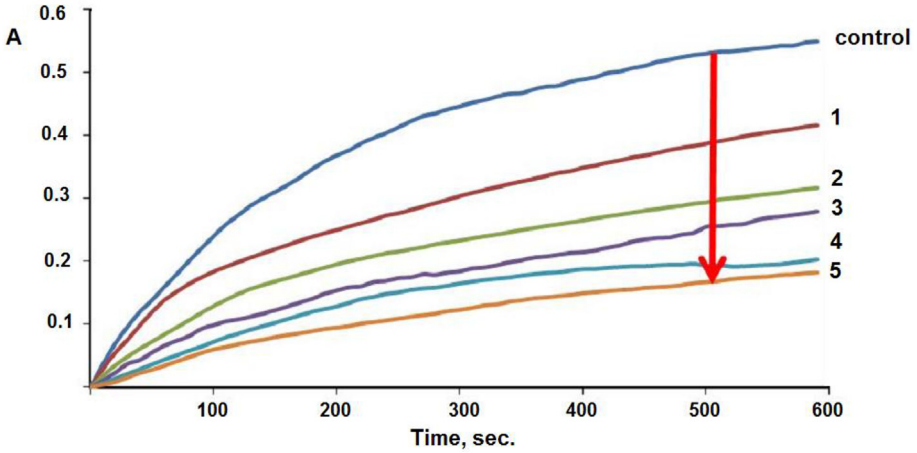

Fig. 6. Kinetic curves of LA oxidation by LOX-1B at different concentrations of Co complex **4**. (1–1 μM; 2–5 μM; 3–10 μM; 4–25 μM; 5–50 μM, borate buffer pH 9.0).

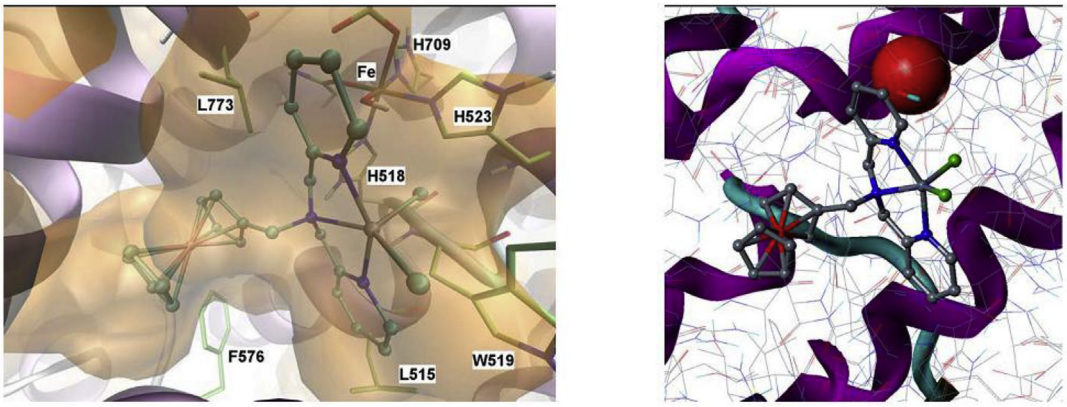

Fig. 7. The docked pose of 6 in the fatty acid binding site of LOX-1.

rat brain homogenates (RBH). Lipid peroxidation induced by Fe^{3+}-ions ($FeNH_4(SO_4)_2 \cdot 12H_2O$) or by *tert*- butylhydroperoxide (^tBHP). The LP level was monitored spectrophotometrically by the concentration of thiobarbituric acid reactive substances (TBARS) at λ_{max} 532 nm. The content of TBARS derived from $(A_0 - A_1)/A_0 \cdot 100\%$, where A_0 - optical density of blank probe with only diluent, A_1 - optical density of probe with additive, is shown in Table 5.

The complexes **2**–**6** inhibiting ^tBHP induced lipid peroxidation efficiently. The activity of cobalt and manganese complexes is lower than that of ligand **1**. In the presence of Fe complex **3** the level of lipid peroxidation increased. It seems to be related to oxidation $Fe^{II} \rightarrow Fe^{III}$ in the complex, which could additionally promote LP.

Table 5
Effect of **1**–**6** (30 μM) on induced lipid peroxidation of rat brain homogenates, estimated as TBARS, and the rat cerebral cortex neuron survival after 20 h of incubation with 1 μM of **1**–**6** determined by MTT method.

Compound	^tBHP-induced LP (% of control)	IC_{50}, μM	Neuron survival, %
1	21.9	0.32 ± 0.03	63 ± 10
2	8.3	0.27 ± 0.02	61 ± 10
3	[a]	–	99 ± 10
4	36.7	0.77 ± 0.05	86 ± 38
5	39.5	0.32 ± 0.03	61 ± 29
6	14.9	0.35 ± 0.02	64 ± 19

[a] Complex **3** demonstrated pro-oxidant activity – the peroxidation level was 143% higher than that of control experiment.

2.15. MTT test

The toxicity of **1**–**6** was studied on primary cultures of brain cortex and hippocampus of rat neurons obtained from newborn rats (1–2 days) by trypsinization followed by pipetting [47]. Experiments were performed on 8–10 days cultures. In order to study the effect of **1**–**6** on the cell survival, the primary culture of rat cortical neurons was incubated for 24 h at 37 °C in cell medium. MTT assay was performed on the next day by the standard procedure [48]. The data obtained are shown in Table 5. Neuronal survival was at least 60% under the conditions of the experiment, the Fe (99%) and Co (86%) complexes demonstrating the lowest toxicity. Compounds **1**–**6** are promising antioxidants due to a sufficiently low toxicity and their high efficiency in a number of antioxidant activity assays.

3. Conclusions

The synthesis, structures, redox properties and *in vitro* antioxidant effects of a series of new Cu, Fe, Co, Mn, Zn, complexes with ferrocenylmethylbis (2-pyridylmethyl)amine is presented. The metal complexes **2**–**6** are polytopic agents since their molecules possess two redox-active centers (ferrocenyl group and dipicolylamine complex) capable of electron transfer. The electrochemical study demonstrates that all these compounds are redox-active ones and the independent redox transitions involving ferrocenium

moiety, dipicolylamine and metal ion take place.

The antioxidant radical scavenging activity of complexes was measured using DPPH test and linoleic acid peroxidation. Although most compounds are weak antioxidants, high activity was found for easily oxidized Fe complex as well as for its analogue containing antioxidant 2,6-di-*tert*-butylphenol group [14].

In electron transfer reactions (CUPRAC test and inhibition of enzymatic generation of superoxide radical-anion by xanthine oxidase) Mn complexes show greater activity than the other metal complexes. The LOX-1B inhibition activity of the studied compounds was evaluated, with all complexes showing $IC_{50} < 50$ μM. The *in vitro* experiments with rat brain homogenate indicate high antioxidant activity of all the compounds in inhibition of ^{t}BHP induced lipid peroxidation. These results let us to conclude that combining in one molecule several redox active metal centers is a promising way of metallodrug design in modern medicinal chemistry.

4. Experimental

4.1. Materials and equipment

Ferrocenylmethyltrimethylammonium iodide was synthesized as described previously [49], di-(2-picolyl)amine (Aldrich, 97%), $ZnCl_2 \cdot 2H_2O$, anhydrous $MnCl_2$, $FeCl_2$, $CoCl_2$, $NiCl_2$, $CuCl_2$ were used. Solvents (DMF, diethyl ether, petroleum ether, methanol, acetone, ethanol) were used as supplied (without further purification).

Infrared spectra were recorded in KBr pellets with "IR200 Thermo Nicolet" spectrometer. Electronic absorption spectra were measured on "Evolution 300 Termo Scientific" spectrophotometer. The NMR measurements were performed with a Bruker Avance-400 spectrometer operating on 400.1 (^{1}H) and 100.6 MHz (^{13}C) in $CDCl_3$. The MALDI TOF spectra were acquired using Autoflex II (Bruker daltonics) mass spectrometer. The samples were dissolved in $CHCl_3$ and put at target.

4.2. Synthesis

4.2.1. Ferrocenylmethyl-bis(2-pyridylmethyl)amine 1 (L)

Mixture of 1.16 g (3 mmol) of ferrocenylmethyltrimethylammonium iodide and 1.08 ml (6 mmol) of di-(2-picolyl) amine in 1 ml DMF in a Schlenk vessel was heated for 2 h at 110–115 °C under argon. To the reaction mixture after cooling to room temperature 10 ml of water were added and it was extracted by diethyl ether (5 × 5 ml). The ether extracts were combined and the solvent evaporated in vacuo (10 mm Hg) to a minimum volume. The residue was allowed to crystallize for 24 h, the resulting orange crystals were washed with cold petroleum ether, and dried in air for a day. Yield 82%. Mp 73°C.

IR (cm^{-1}): 1566, 1587, 3082-2908 ($\nu_{C\text{-}H}$ cm^{-1}).

^{1}H-NMR (δ(ppm), $CDCl_3$): 3.56 (s, 2H, FcCH_2N); 3.76 (s, 4H, N(CH_2)$_2$); 4.01 (s, 5H, Fc); 4.09 (d, 2H, Fc); 4.19 (d, 2H, Fc); 7.12 (dd, 2H, $J_{нн}$ = 8 Hz, 4 Hz, 2Py); 7.52 (d, 2H, $J_{нн}$ = 8 Hz, 2Py); 7.63 (td, 2H, $J_{нн}$ = 8 Hz, 2 Hz, 2Py); 8.51 (d, 2H, $J_{нн}$ = 4 Hz, Py).

^{13}C-NMR: 53.56, 54.76, 59.43, 68.41, 70.14, 82.74, 121.82, 122.76, 136.33, 148.88, 160.06.

UV–vis spectrum (MeOH), λ_{max}, nm (lgε): 262.0 (4.1), 432.0 (2.3); UV–vis spectrum (CH_2Cl_2) λ_{max}, nm (lgε): 229.0 (3.9), 257.0 (3.9), 436.0 (2.2).

4.2.2. [$CuCl_2$L] (**2**)

Cu complex **2** was obtained according to the method described previously [33]. To a solution of 50 mg **L** (0.126 mmol) in 0.5 ml MeOH, $CuCl_2$ (17 mg, 0.126 mmol) in 0.5 mL of methanol was added under stirring. The green solution was left for 24 h. The crystalline solid was washed with petroleum ether and dried on the air. Yield 70%, Mp > 250°C.

IR (cm−1): 1574, 1610, 3030, 3066, 3086, 2914, 2941, 2952.

MS (MALDI TOF), *m/z*: [L·CuCl]$^{+}$- 495, [L_2 Cu_2Cl_3]$^{+}$- 1027.

UV–vis spectrum (EtOH), λ_{max}, nm, (lgε): 259.0 (4.2), 442.5 (2.3), 677.5 (2.3); UV–vis spectrum (CH_2Cl_2), λ_{max}, nm (lgε) 229.5 (4.2), 258.0 (4.2), 462.5 (2.4), 763.0 (2.4).

4.2.3. General procedure for the preparation of complexes (3–6)

To a solution of 200 mg **L** (0.5 mmol) in 2 ml of acetone 0.5 mmol of metal chloride was added under stirring. The mixture was stirred for 30 min, and the precipitation of complexes was observed. The crystals of complex were filtered off, washed with cold petroleum ether and dried in vacuo. The yields were 50–60%.

[FeCl2L] (3) Yellow green powder. Yield 52%. Mp > 250 ◦C. Anal. calcd: C 52.72%, H 4.42%, N 8.02%. Found: C 52.60%, H 4.50%, N 7.91%.

IR (KBr, cm^{-1}): 1572, 1605, 3026, 3082, 2908, 2936.

^{1}H-NMR (δ(ppm), $CDCl_3$): 3.57 (s, 2H, FcCH_2N); 3.77 (s, 4H, N(CH_2)$_2$); 4.03 (s, 5H, Fc); 4.11 (d, 2H, Fc); 4.20 (d, 2H, Fc); 7.14 (dd, 2H, $J_{нн}$ = 8 Hz, 4 Hz, 2Py); 7.55 (d, 2H, $J_{нн}$ = 8 Hz, 2Py); 7.65 (td, 2H, $J_{нн}$ = 8 Hz, 2 Hz, 2Py); 8.53 (d, 2H, $J_{нн}$ = 4 Hz, Py).

^{13}C-NMR: 53.57, 59.41, 67.98, 68.43, 70.16, 82.70, 121.86, 122.77, 136.38, 148.95, 160.04.

MS (MALDI TOF), *m/z*: [L · FeCl]$^{+}$ - 488; [(L)$_2$ · Fe_2Cl_3]$^{+}$ - 1011, 1013.

UV–vis spectrum (EtOH), λ_{max}, nm (lgε): 253.5 (4.1), 375.5 (3.4); UV–vis spectrum (CH_2Cl_2), λ_{max}, nm (lgε), 255.5 (4.0), 385.5 (3.3).

[$CoCl_2$L] (4). Brown powder. Yield 57%. Mp. >250 °C. Anal. calcd: C 52.41%, H 4.40%, N 7.97%. Found: C 52.31%, H 4.46%, N 8.14%.

IR (cm^{-1}): 1572, 1606, 2999, 3030, 3076, 2854, 2917.

MS (MALDI TOF), *m/z*: [L · CoCl]$^{+}$ - 491; [L_2 · Co_2Cl_3]$^{+}$ - 1017, 1019.

UV–vis spectrum (EtOH), λ_{max}, nm (lgε): 257.5 (4.2), 591.5 (2.4); UV–vis spectrum (CH_2Cl_2), λ_{max}, nm (lgε)228.0 (4.0), 256.5 (3.9), 418.5 (2.2), 523.0 (2.2), 557.5 (2.2), 636.5 (2.1).

[$MnCl_2$L] (5). Yellow powder. Yield 60%. Mp > 250 °C.

Anal. calcd: C 52.81%, H 4.43%, N 8.03%. Found: C 52.62%, H 4.51%, N 7.95%.

IR (KBr pellet, cm^{-1}): 1572, 1603, 3074, 3093, 2918, 2960, 2987.

MS (MALDI TOF), *m/z*: [L · MnCl]$^{+}$ - 487; [(L)$_2$ · Mn_2Cl_3]$^{+}$ - 1009, 1011.

UV–vis spectrum (EtOH), λ_{max}, nm (lgε): 261.0 (4.1), 428.5 (2.3); UV–vis spectrum (CH_2Cl_2), λ_{max}, nm (lgε), 227.5 (4.0), 262.5 (4.0).

[$ZnCl_2$L] (6). The synthesis and analysis were described in detail in Ref. [46].

4.2.4. Crystallographic data collection and structure determination of complex 6

In order to obtain crystals of the Zn complex to the **L** solution (50 mg, 0.126 mol) in 100 mL of MeOH, 22 mg of $ZnCl_2 \cdot H_2O$ in 0.35 ml MeOH were added, than the mixture was left in the air and after some time needle-like crystals appeared. All diffraction data were collected on an Enraf Nonius CAD-4 diffractometer [λ(MoKα) = 0.71073 Å, ω-scans] at 293 K. The transparent crystals of complex **6** were selected for the experiment. The unit cell parameters were refined from 25 reflections. The structure was solved by direct methods using the software package SIR2002 CC [50]. The structure was refined by the full-matrix least-squares technique against F in the anisotropic–isotropic approximation using the software package JANA2000 CC [51]. Some of the hydrogen atoms were found from difference Fourier synthesis, the rest position is calculated from the geometry of the molecule. The refinement of hydrogen atoms initially was produced in conjunction with the respective carbon atoms at a distance of 1.04 Å and angles

corresponding to the type of hybridization of carbon atoms. Parameter of hydrogen atomic displacement was assumed to be 1.2 of the corresponding carbon atoms atomic displacement. At the final stage, these restrictions were removed, and the hydrogen atoms were refined independently. Crystal data and structure refinement parameters are listed in Supporting Materials (Appendix A. Table S1). CCDC 1486751 contains the supplementary crystallographic data for this paper.

4.2.5. Antioxidant activity studies

DPPH radical scavenging activity, lipoxygenase activity, CUPRAC assay (Cu^{2+} reducing), inhibition of superoxide radical anion formation by xanthine oxidase (NBT assay), inhibition of LA peroxidation and inhibition of Fe^{3+} and ^{t}BHP induced lipid peroxidation studies were performed according the procedures described in Ref. [14]. DPPH, lipoxidase (LOX 1-B) from Glycine max (soybean), linoleic acid (Sigma-Aldrich 99%), xanthine oxidase were purchased from Sigma-Aldrich.

4.2.6. Electrochemical study

All measurements were carried out under argon at room temperature. Cyclic voltammetry experiments were performed in classical three-electrode cell in CH_3CN solution with 0.05 M Bu_4NBF_4 as supporting electrolyte using a model IPC-Win potentiostat. The number of electrons transferred were determined by comparing with the height of Fc^{2+}/Fc^{3+} wave for the same concentration and by rotating disk electrode method as well. A platinum or glassycarbon (GC) working electrode with diameter 2 mm, platinum wire auxiliary electrode and aqueous Ag/AgCl/KCl (sat.) reference electrode were used. The solvents were routinely distilled and dried prior to use [52].

4.2.7. Molecular docking

The structure of complex **6** was extracted from the CIF file and optimized using PM6 semiempirical method [53] in MOPAC2009 [54] via SYBYL8.0 interface [55]. Preparation of the initial structure for docking was performed in MGLTools 1.5.4 [56]; ferrocene was represented as a rigid structure with 10 Fe-C bonds, two bonds of the linker were marked as rotatable, and the rest of the structure was represented as rigid. PM6 charges were used for docking as recommended [57]. Autodock 4.2 [58,59] was used for docking the complex into previously prepared [60] LOX model based on PDB [61] structure 1IK3 [62]; 100 docking solutions were generated and analyzed visually with MGLTools and SYBYL, and 98 of them gave the solution depicted at Fig. 7.

Acknowledgements

The financial support from Russian Foundation for Basic Research (Grants № 15-03-03057, 17-03-00892) is gratefully acknowledged. The biological studies were performed with support of Russian Science Foundation (Grant № 14-13-00483).

Appendix A. Supplementary data

Supplementary data related to this article can be found at http://dx.doi.org/10.1016/j.jorganchem.2017.03.036.

References

[1] B. Park, S. Lee, E. Lee, et al., J. Mol. Struct. 890 (2008) 123–129.
[2] Y. Kim, B. Park, G. Eom, S. Kim, H. Park, Y. Choi, H. Jang, Ch. Kim, Inorg. Chim. Acta 366 (2011) 337–343.
[3] E. Tomat, S. Lippard, Curr. Opin. Chem. Biol. 14 (2010) 225–230.
[4] S. Kim, J. Hong, Tetrahedron Lett. 50 (2009) 2822–2824.
[5] C. Kulatilleke, S. de Silva, Y.A. Eliav, Polyhedron 25 (2006) 2593–2596.
[6] Q. Zheng, S. Chen, Z. Wang, Y. Cui, Talanta 85 (2011) 824–828.
[7] X. He, N. Zhu, V.W. Yam, Organometallics 28 (2009) 3621–3624.
[8] C. Park, J. Hong, Tetrahedron Lett. 51 (2010) 1960–1962.
[9] R. Hanshaw, S. Hilkert, H. Jiang, B. Smith, Tetrahedron Lett. 45 (2004) 8721–8724.
[10] H. Rhee, K. Kim, P. Han, J. Hong, Bioorg. Med. Chem. Lett. 20 (2010) 1145–1147.
[11] F. Ba, F. Robin-Le Guen, N. Cabon, P. Le Poul, S. Golhen, N. Le Poul, B. Caro, J. Organomet. Chem. 695 (2010) 235–243.
[12] G. Gasser, C. Mari, M. Burkart, S.J. Green, J. Ribas, H. Stoeckli-Evansy, J.H.R. Tucker, NewJ. Chem. 36 (2012) 1819–1827.
[13] N.N. Meleshonkova, D.B. Shpakovsky, A.V. Fionov, A.V. Dolganov, T.V. Magdesieva, E.R. Milaeva, J. Organomet. Chem. 692 (2007) 5339–5344.
[14] E.R. Milaeva, D.B. Shpakovsky, Y.A. Gracheva, S.I. Orlova, V.V. Maduar, B.N. Tarasevich, N.N. Meleshonkova, L.G. Dubova, E.F. Shevtsova, Dalton Trans. 42 (2013) 6817–6828.
[15] J.L. Pierre, M. Fontecave, BioMetals 12 (1999) 195–199.
[16] E.-J. Shin, K. Ho Ko, W.-K. Kim, J.S. Chae, T.P.H. Yen, H.J. Kim, M.-B. Wie, H.-C. Kim, Neurochem. Int. 52 (2008) 1134–1147.
[17] B. Halliwell, J.M.C. Gutteridge, Free Radicals in Biology and Medicine, Oxford University Press, Oxford, U.K, 2007, p. 851.
[18] W. Droge, Free radicals in the physiological control of cell function, Physiol. Rev. 82 (2002) 47–80.
[19] Zai-Qun Liu, Chem. Rev. 110 (2010) 5675–5691.
[20] E. Niki, Free Radic. Biol. Med. 49 (2010) 503–515.
[21] R. Scherer, H.T. Godoy, Food Chem. 112 (2009) 654–658.
[22] V. Bondet, W. Brand-Williams, C. Berset, Food Sci. Technol. 30 (1997) 609–615.
[23] W. Brand-Williams, M.E. Cuvelier, C. Berset, Food Sci. Technol. 28 (1995) 25–30.
[24] R. Apak, K. Guglu, M. Ozyurek, S. Karademir, J. Agric. Food Chem. 52 (2004) 7970–7981.
[25] K. Mishra, H. Ojha, N.K. Chaudhury, Food Chem. 130 (2012) 1036–1043.
[26] Q.P. Sharma, T.K. Bhat, Food Chem. 113 (2009) 1202–1205.
[27] A.M. Pisoschi, C. Cimpeanu, G. Predoi, Open Chem. 13 (2015) 824–856.
[28] V.Yu. Tyurin, N.N. Meleshonkova, A.V. Dolganov, A.P. Glukhova, E.R. Milaeva, Russ. Chem. Bul. 60 (2011) 647–655.
[29] V.Yu. Tyurin, Z. Jingwei, A. Glukhova, E.R. Milaeva, Macroheterocycles 4 (2011) 211–212.
[30] V.Yu. Tyurin, Wu Yaohuan, A.V. Dolganov, E.R. Milaeva, Dokl. Chem. 436 (2011) 31–33.
[31] S. Chevion, M.A. Roberts, M. Chevion, Free Radic. Biol. Med. 28 (2000) 860–870.
[32] V.Yu. Tyurin, A.A. Moiseeva, D.B. Shpakovsky, E.R. Milaeva, J. Electroanal. Chem. 756 (2015) 212–221.
[33] A. Evans, S. Watkins, D. Craig, S. Colbran, J. Chem. Soc. Dalton Trans. (2002) 983–994.
[34] E. Ruehl, A.P. Hitchcock, K. Carbon, J. Am. Chem. Soc. 111 (1989) 5069–5075.
[35] J. Frey, L. Du Pont, J. Puckett, J. Org. Chem. 59 (1994) 5386–5392.
[36] S. Fukuzumi, S. Mochizuki, T. Tanaka, Inorg. Chem. 28 (1989) 2459–2465.
[37] H. Lund, O. Hammerich, Organic Electrochemistry, Marcel Dekker, New York, Basel, 2001, p. 1393.
[38] N. Dwadnia, F. Allouch, N. Pirio, J. Roger, H. Cattey, S. Fournier, M.-J. Penouilh, C.H. Devillers, D. Lucas, D. Naoufal, R. Ben Salem, J.-C. Hierso, Organometallics 32 (2013) 5784–5797.
[39] C.K. Mann, K.K. Barnes, Marcel Dekker, New York, 1960 (560 pp.).
[40] A.G. Majouga, O.V. Shilova, A.A. Moiseeva, N.V. Zyk, E.K. Beloglazkina, Rus. Chem. Bull. Int. Ed. 58 (2009) 1392–1399.
[41] E.K. Beloglazkina, A.V. Shimorsky, A.G. Mazhuga, O.V. Shilova, V.A. Tafeenko, N.V. Zyk, Russ. J. Gen. Chem. 79 (2009) 1504–1508.
[42] E.K. Beloglazkina, A.V. Shimorsky, A.G. Majouga, A.A. Moiseeva, N.V. Zyk, Russ. Chemi. Bull. 56 (2007) 2189–2199.
[43] I. Kubo, N. Masuoka, T. Ha, K. Tsujimoto, Food Chem. 99 (2006) 555–562.
[44] S. Zhang, J. Wang, L. Han, C. Li, W. Wang, Z. Yuan, Sens. Actuators, B Chem. 147 (2010) 687–690.
[45] A. Andreou, I. Feussner, Phytochem 70 (2009) 1504–1510.
[46] E.R. Milaeva, N.N. Meleshonkova, D.B. Shpakovsky, V.V. Pavlovets, S.I. Orlova, D.I. Osolodkin, V.A. Palyulin, S.V. Loginov, P.A. Storoghenko, N.S. Zefirov, Dokl. Chem. 443 (2012) 77–79.
[47] A. Shahar, A Dissection and Tissue Culture Manual of the Nervous System, Wiley-Liss, New York, 1989, pp. 203–206, 371.
[48] M. Niks, M. Otto, J. Immunol. Methods 130 (1990) 149–151.
[49] D. Lednicer, C.R. Hauser, Org. Synth. 40 (1960) 31–33.
[50] M. Burla, M. Camalli, B. Carrozzini, G. Cascarano, C. Giacovazzo, G. Polidori, R. Spagna, SIR2002: the program, J. Appl. Cryst. 36 (2003) 1103.
[51] V. Petricek, M. Dusek, L. Palatinus, Structure Determination Software Programs, Institute of Physics, Praha, Czech Republic, 2000.
[52] A.J. Gordon, R.A. Ford, The Chemist's Companion: a Handbook of Practical Data, Techniques and References, Wiley, New York, 1972, p. 422.
[53] J.J.P. Stewart, J. Mol. Model 13 (2007) 1173–1213.
[54] J.J.P. Stewart, Stewart Computational Chemistry, Version 11.038L. web: HTTP://OpenMOPAC.net.
[55] SYBYL8.0,Tripos International, 1699 South Hanley Rd., St. Louis, Missouri, 63144, USA.
[56] M.F. Sanner, J. Mol. Graph. Model 17 (1999) 57–61.

[57] Z. Bikadi, E. Hazai, J. Cheminf 1 (2009) 15.
[58] G.M. Morris, D.S. Goodsell, R.S. Halliday, R. Huey, W.E. Hart, R.K. Belew, A.J. Olson, J. Comput. Chem. 19 (1998) 1639–1662.
[59] R. Huey, G.M. Morris, A.J. Olson, D.S. Goodsell, J. Comput. Chem. 28 (2007) 1145–1152.
[60] E.R. Milaeva, S.I. Orlova, D.I. Osolodkin, V.A. Palyulin, E.Y. Fursova, V.I. Ovcharenko, N.S. Zefirov, Russ. Chem. Bull. 60 (2011) 2564–2571.
[61] H.M. Berman, J. Westbrook, Z. Feng, G. Gilliland, T.N. Bhat, H. Weissig, I.N. Shindyalov, P.E. Bourne, Nucleic Acids Res. 28 (2000) 235–242.
[62] E. Skrzypczak-Jankun, R.A. Bross, R.T. Carroll, W.R. Dunham, M.O. Funk Jr., J. Am. Chem. Soc. 123 (2001) 10814–10820.